Giant spin splitting, strong valley selective circular dichroism and valley-spin coupling induced in silicene

Jinfeng Qu, Xiangyang Peng, Di Xiao, and Jianxin Zhong

Phys. Rev. B **94**, 075418 — Published 15 August 2016

DOI: 10.1103/PhysRevB.94.075418

Giant spin splitting, strong valley selective circular dichroism and valley-spin coupling induced in silicene

Jinfeng Qu,[1] Xiangyang Peng,[1*] Di Xiao,[2] Jianxin Zhong[1†]

[1]*Hunan Key Laboratory of Micro-Nano Energy Materials and Devices, Xiangtan University, Hunan 411105, P.R. China*

[2]*Department of Physics, Carnegie Melon University, Pittsburgh, Pennsylvania 15213, USA*

Abstract

Silicene is a potential candidate for valleytronics. However, in comparison with the transition metal dichalcogenides, silicene has a tiny energy gap and zero spin splitting at its Dirac valleys, being unfavorable for valleytronic applications. Based on first principles calculations, we find that by proximity with Bi(111) bilayer, the Dirac valleys of silicene acquire a sizable energy gap and giant spin splittings, which are even larger than the splittings of MoS_2. Our calculations show that the silicene over Bi layer exhibits a strong valley-contrasting circular dichroism, enabling selective optical pumping of valley carriers. Due to the time reversal symmetry and the breaking of inversion symmetry, the Berry curvatures and the spin-splittings are opposite at the K and K′ valleys of silicene, and hence the valley and spin are locked and can be simultaneously polarized. In this way, silicene and likely other similar Dirac materials can be comparable to transition metal dichalcogenides in valleytronics, which not only adds a new dimension to the properties of silicene but also expands the members of valleytronic family.

PACS Numbers: 73.20.-r, 74.45.+c, 71.70.Ej, 78.67.-n

I. INTRODUCTION

Using electrical charge to process information is approaching its thermodynamic and quantum limits. Spintronics is a promising solution to circumvent these fundamental limits by encoding information with the spin of electrons [1]. In principle, other quantum degrees of freedom can also be utilized for information coding in addition to spin. Wave number is a quantum number related to the momentum of electrons in crystalline solids. In the Brillouin zone of some materials, such as graphene, silicene, diamond, bismuth and silicon, there are multiple energy valleys locating at some special k points [2-7]. In parallel to spintronics, valleytronics soon arises and becomes a fascinating and fast growing field, aiming to encode information by harnessing the valley carriers that carry these special momenta [2,4,8-11]. Up to present, however, only ultrathin transition-metal dichalcogenides (TMDs) are distinguished as exceptional among all valleytronic materials, and hence most of current researches are focused on TMDs [12-15]. Monolayer TMDs such as MoS_2 and WSe_2 have strong spin orbit coupling (SOC), valley-contrasting Berry curvatures and giant spin-orbit splittings. The interplay of valley, spin and the Berry-phase related physics in TMDs has aroused immense interest [16,17].

Beyond TMDs, the weak SOC Dirac materials such as silicene are also candidates for valleytronics. Compared with TMDs, they are featured by very large coherence length, dissipationless ballistic carrier transport, bipolar transistor effect, exceptionally high charge mobility[18,19] and thermal conductivity [20]. Silicene has two valleys, i.e., Dirac cones, at the K and K′ points of the Brillouin zone. However, silicene is not comparable with TMDs in terms of valleytronic properties, because the almost gapless Dirac valleys of silicene are not suitable for switching applications, and the very weak SOC and inversion symmetry in silicene suppress the coupling of valley and spin. It would be desirable to introduce an appreciable band gap and large SOC in silicene so that it can emulate TMDs in valleytronics.

By performing first-principles calculations, we demonstrate that this can be achieved by forming heterostructures with strong SOC materials, such as Bi(111) bilayers [21]. Bi bilayers have been successfully grown in experiments[22,23]. Silicene has also been synthesized on different substrates, such as Ag[24-26], Ir[27], $ZrBr_2$[28] and ZrC[29]. In particular, a growth–transfer–fabrication technology is developed[30], which can potentially be used to realize various silicene heterostructures, including silicene/Bi(111). Our calculations find that silicene can acquire giant spin splittings from the Bi(111) bilayer by proximity effect, and the interaction with Bi layer opens a considerable gap at the Dirac valleys of silicene. The spin-splittings and the Berry curvatures are confirmed to be valley contrasting. Therefore, we can integrate by this approach

the new valleytronic properties, e.g., the valley selective circular dichroism, valley Hall effects and spin-valley locking, with the existing excellent properties of silicene.

II. COMPUTATIONAL METHODS

In the framework of density functional theory, the calculations are performed by using Vienna ab-initio simulation package within the generalized gradient approximation with van der Waals corrections [optimized Perdew-Burke-Ernzerhof-vdW (optB88-vdW)] [31-33]. Projector augmented wave (PAW) potentials are employed to describe the electron-core interaction [34]. The energy cutoff for planewave expansion is set to be 400 eV and the Brillouin zone is sampled by a Γ-centered $6\times6\times1$ grid. SOC is always taken into consideration unless otherwise stated. The composite system of monolayer silicene and Bi bilayer is modeled by periodic slabs, which are separated by a vacuum of 15Å to decouple the periodic images. During structural relaxation, all atoms are allowed to move until the forces on each atom are smaller than 0.02eV/Å. These computational settings have led to good convergence in the calculations. The Berry curvatures are calculated by using Wannier90 [35]. Since the system studied does not possess inversion symmetry, we used a Z2pack code to calculate the Z_2 index, which is based on the scheme proposed by Alexey A. Soluyanov and David Vanderbilt[36].

III. RESULTS AND DISCUSSION

We started by calculating the pristine monolayer silicene and Bi(111) bilayer, whose experimental lattice constants are 3.866Å and 4.52Å, respectively. Our calculations show that the Si atoms are alternately up and down in silicene with a buckling of 0.44 Å between the upper and lower Si atoms. The bands have a tiny SOC gap of 1.2 meV at the Dirac valleys. The calculated Bi(111) bilayer is 1.66 Å thick and possesses a direct SOC gap of 0.57 eV at the Γ point. Our calculated atomic and electronic structures of pristine silicene and single Bi(111) bilayer agree with the previous calculations very well [37-39].

The heterostructure of the monolayer silicene and single Bi(111) bilayer is modeled by silicene-(2×2) over Bi(111)-($\sqrt{3}\times\sqrt{3}$)$R30^\circ$ as shown in Fig. 1(a) and (b), in which the lattice mismatch is as small as 1.2%. For brevity in the following discussion, this system will be denoted by Si/Bi. When we mention silicene and Bi layer, we always mean the monolayer silicene and single Bi(111) bilayer, respectively. We studied three typical configurations with different stacking registries. It is found that the most stable configuration of Si/Bi

is the one shown in Fig. 1, with a lower Si_1 atom on top of an upper Bi_1 atom, and an upper Si_2 atom on top of another upper Bi_2 atom in the supercell (for the other two configurations, please see Fig. S1 in the supplemental materials). After relaxation, the average buckling of silicene increases from 0.44 Å to 0.48 Å and the thickness of Bi bilayer becomes 1.63Å. Si_1 and Si_2 are pulled down by 0.18 Å and 0.50 Å with respect to other equivalent Si atoms, respectively, and the Bi_1 and Bi_2 atoms below them are pushed down by 0.32 Å, resulting in an average Si-Bi layer separation of 2.91Å and a Si_1-Bi_1 distance of 2.90Å. The large relaxation of the Si_1, Si_2 and Bi_1, Bi_2 atoms and the large charge distribution between Si_1 and Bi_1 atoms [Fig. 1(b)] suggest strong interactions between Si and Bi layers and significant hybridization of the Si and Bi states. We made some random displacements of silicene from its equilibrium position and found that silicene will return to its original equilibrium position after relaxation, indicating that the Si/Bi system shown Fig. 1 is stable with respect to perturbations. The average binding energy per Si atom between silicene and Bi layer is 68 meV, which is much smaller than that between silicene and Ag(111)[40] but appreciably larger than that between silicene and h-BN[41]. The Si/Bi system can possibly be realized by transferring technology. Although the pristine silicene and Bi layer possess inversion symmetry, respectively, there is no common inversion center in Si/Bi. The inversion symmetry is apparently broken along the z direction and the in-plane inversion symmetry also vanishes due to the lack of x-mirror.

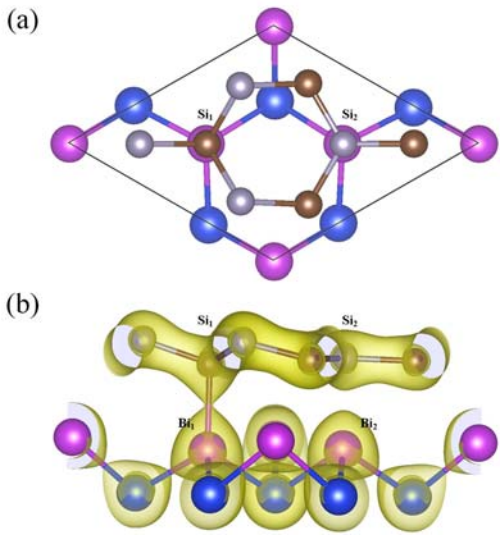

FIG. 1 (Color online). The top (a) and the side (b) views of the optimized Si/Bi system. The gray and brown spheres denote the upper and lower Si atoms in the buckled silicene, and the purple and blue spheres represent the upper and lower Bi atoms in Bi(111) bilayer, respectively. Si_1 and Si_2 denote the lower Si atom and the upper Si atom that are right above the top of the upper Bi_1 and Bi_2 atoms, respectively. The isosurface plotting of the total charge distribution is also given in (b).

The calculated electronic bands of the Si/Bi heterostructure are shown in Fig. 2(a), which can basically be viewed as the superposition of the bands of the isolated silicene [Fig. 2(b)] and Bi layer [Fig. 2(c)]. However, the Si-Bi interaction has resulted in appreciable modifications. The Dirac valleys of silicene at K and K′ are preserved in the composite system whereas the gap of the valleys is radically increased from 1.2 meV to 44 meV. Bi atoms have very strong SOC and with the breaking of the inversion symmetry in Si/Bi, one would expect the occurrence of spin-splitting. What is unexpected is the giant magnitude of the spin splitting near the Dirac valleys of silicene, as shown in Fig. 2(a). We denote the valley spin splittings in the valence and conduction band edges by Δ_{KV} and Δ_{KC}, respectively (Fig. 2(a)). With a surprisingly large magnitude of 170 meV, the Δ_{KV} of Si/Bi is even greater than the Δ_{KV} of MoS_2 by about 20 meV [42], signifying that the proximity effect has significantly enhanced the SOC in silicene adlayer. Notably, the Δ_{KC} of Si/Bi (100 meV) is at least three times larger than that of TMDs, which ranges from 3 meV for MoS_2 and 36 meV for WSe_2[42,43]. In Si/Bi, the Δ_{KC} and Δ_{KV} are of similar scale whereas in TMDs, they are highly asymmetric with Δ_{KC} smaller than Δ_{KV} by at least one order [42]. Another salient feature is that the spin splittings are opposite at the K and K′ valleys. As shown in Fig. 2(a), the top valence band edge at K has down spins whereas that at K′ point has up spins. The Bloch states at K and K′ valleys form a Kramer's pair and the time reversal symmetry dictates the valley contrasting spin splittings, which sets the basis for coherent manipulation of spin and valley freedoms as will be discussed below. Different from the in-plane Rashba-type spin polarization, it is found that the spin vector at the Dirac valleys is almost normal to the surface plane of silicene, which is of the same type of the Zeeman splitting found in bilayer WSe_2 induced by electric field [44]. But here in Si/Bi, neither magnetic nor electric fields are required. The in-plane components of the spin at Dirac valleys is very small, but are still valley contrasting. Γ and M points are the only time reversal invariant k points, where the opposite spin states have to be degenerate. Therefore, the spin-up and spin-down bands cross at the Γ and M points [Fig. 2(a)], leading to Rashba-like splittings around these two points.

To the best of our knowledge, the giant magnitude of spin splitting shown above is by far the largest one ever been found in silicene, e.g., by application of electric field or by doping transition metal atoms [45,46]. To understand the giant spin splittings, we project the Bloch wave function onto each ion. Due to the strong interaction as indicated by the large atomic relaxation and the charge distribution along Si_1-Bi_1 (Fig. 1), it is found that the Bi_p states are significantly mixed with the Dirac valley states, as shown in Fig. 2(d) and 2(e). About 50% of the valence band (VB) and conduction band (CB) band edge states of the Dirac valleys are contributed by the Si_p_z orbitals and the other 50% by the Bi_p orbitals. For the valence band edge at the

valleys, the p_z orbitals of the upper Si atoms in the buckled silicene give significant contribution whereas the lower Si atoms almost do not contribute. For the conduction band edge at the valleys, the p_z orbitals of the lower Si atoms give significant contribution whereas the upper Si atoms almost do not contribute. The Bi atoms contribute not only p_z orbitals, but also p_x and p_y orbitals to the valley states. In the upper layer of Bi bilayer, only the Bi_1 and Bi_2 contribute to the conduction and valence valley states, respectively. The lower layer of Bi bilayer have significant contribution to both the valence and conduction valley states. The contribution of the Si and Bi states to the bands is shown in the Fig. S2 of the supplemental materials. The hybridization between the Si_p and Bi_p orbitals in Si/Bi is strong almost throughout the Dirac cone centered at K or K′ point. Since the Bi_p states are the leading source of the strong SOC, Bi_p orbitals induce large spin splittings at the Dirac cone. The highest occupied states around Γ point are mainly from Bi_p orbitals. Since the inversion symmetry is broken in Si/Bi, large spin splitting also occurs near the gamma point. In MoS_2/Bi(111)[47], in contrast, Bi_p states are hybridized with the Mo_d states in the highest occupied states near Γ point but are almost absent at the highest occupied states at K point, resulting large spin splittings near Γ point but very small ones near K point.

For comparison, we also studied the graphene($\sqrt{3}\times\sqrt{3}$)/Bi(1×1) system, where the mismatch is smaller than 2%. It is found that the SOC splitting in the graphene bands is vanishingly small. The monolayer graphene over Bi remains to be flat and the C-Bi separation is calculated to be 3.67 Å, much larger than the Si-Bi separation (<3 Å). There are two factors that may account for the weak graphene-Bi interaction and nearly zero spin-splitting in graphene/Bi. Firstly, the C_2p states are much localized than the Si_3p states and hence the C-Bi hybridization is much smaller than the Si-Bi hybridization. Therefore, the C-Bi interaction is much weaker and C-Bi separation is significantly larger than those in Si/Bi. Secondly, graphene is buckleless and its hybridization and interaction with the substrate are not so effective as the buckled silicene. Since the buckling can enhance the SOC [38], the intrinsic SOC in silicene is considerably stronger than that in graphene. The large Si-Bi interaction and the giant spin splittings are also a result of the direct contact of Si with heavy atoms Bi. To illustrate this, we put one hydrogen atom between Si_1 and Bi_1 and another one between Si_2 and Bi_2 in the configuration shown in Fig. 1. After relaxation, it is found that hydrogen atoms are finally adsorbed on Si_1 and Si_2 atoms (see Fig. S3 in the supplemental materials). The distance between silicene and Bi layers increases from 2.9Å to 4.2Å. Therefore, the interaction between silicene and Bi bilayer is much reduced, and accordingly the spin splitting of VBM and CBM at K is significantly reduced. This test calculation confirms that the spin splitting is sensitively dependent on the Si-Bi separation.

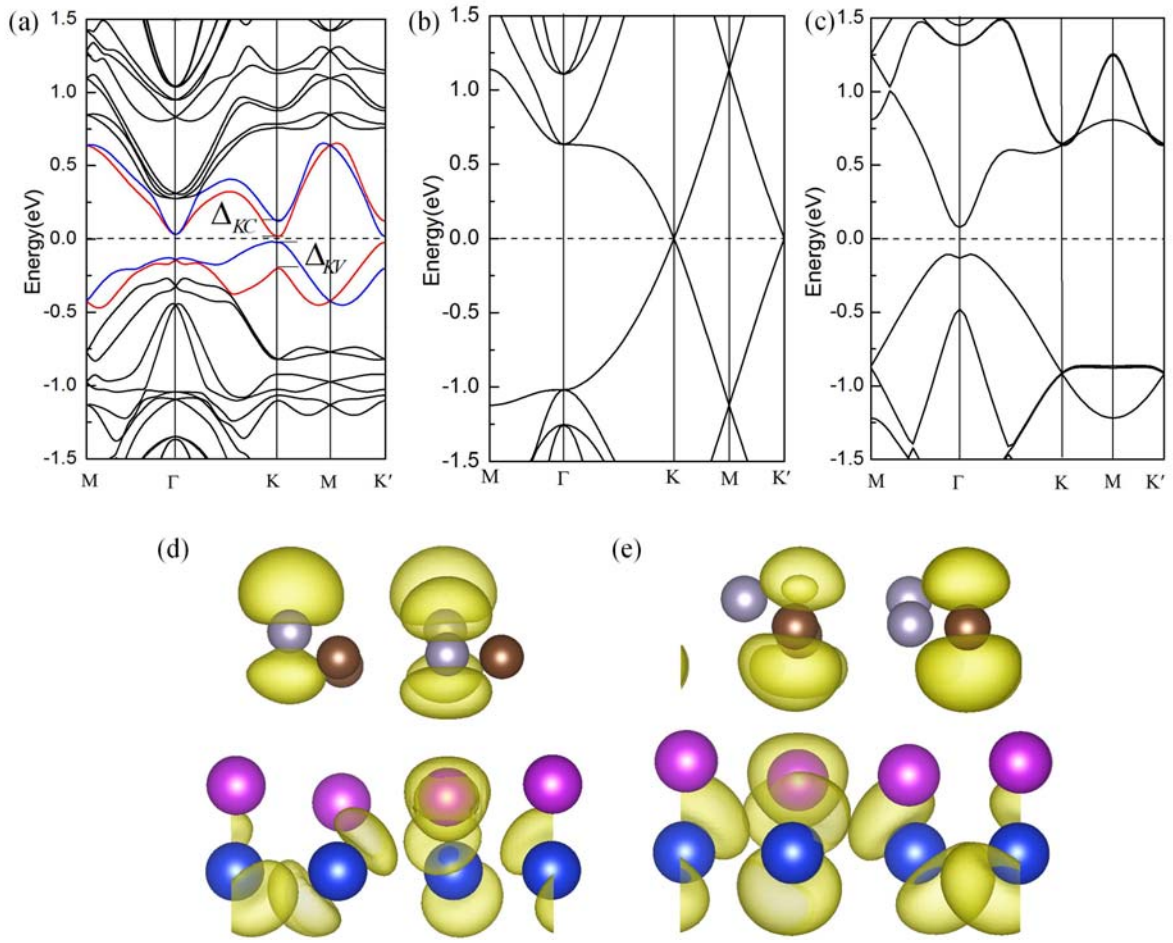

FIG. 2 (Color online). (a) The band structure of Si/Bi. The blue and red colors denote spin-down and spin-up states, respectively. (b) and (c) are the band structures of pristine silicene-(2×2) and Bi(111)-$(\sqrt{3}\times\sqrt{3})R30^{\circ}$ bilayer, respectively. (d) and (e) are the charge distribution of the valence and conduction band edges at K-valley.

To tune the spin splittings and the band gap at the valleys, we applied a 2.7% lateral compressive strain, for instance, to the Si/Bi heterostructure. It is found that the average Si-Bi distance and the buckling of silicene are increased to 2.94 Å and 0.50 Å, respectively. The energy gap is still located at K and K' points, which is significantly widened to 98 meV. The Δ_{KV} is raised to 207 meV while Δ_{KC} is reduced to 35 meV. Therefore, application of strain is an effective approach to modulating the spin splittings and energy gap in the valleys.

We also studied the Z_2 topological phase of the system. Silicene and single Bi(111) bilayer[21,38] are found to be topological insulators (TIs). It might be presumed that the Si/Bi system is also a TI. We calculated

the Z_2 index of Si/Bi by using Z2pack code[36] and found that the Si/Bi system is not a TI.

Now we address the Berry phase effects in Si/Bi. The Berry curvature $\Omega_n(k)$ is an odd function of k in the presence of time reversal symmetry and an even function in the presence of spatial inversion symmetry [8]. Pristine silicene possesses both of the two symmetries and hence $\Omega_n(k)$ vanishes. In Si/Bi, the inversion symmetry is broken by the Si-Bi interaction, allowing nonzero values for $\Omega_n(k)$ and the valley contrasting properties. We calculated the z component of Berry curvatures of the valence bands of Si/Bi $\Omega_{n,z}(k) = -2\mathrm{Im}\left\langle \partial u_{nk}/\partial k_x \middle| \partial u_{nk}/\partial k_y \right\rangle$ [14], where u_{nk} is the periodic part of the Bloch state Ψ_{nk}. It can be seen in Fig. 3(a) that the calculated Berry curvatures of the valence bands at the K and K′ valleys of Si/Bi are nonzero and opposite.

With a sizable energy gap in Dirac valleys and the valley contrasting Berry curvatures obtained, it becomes possible to manipulate the valley quantum freedom by, e.g., the selective optical pumping of the valley carriers in Si/Bi. We calculated the transition matrix element P of circular polarization $P_{\pm}^{cv}(k) = 1/\sqrt{2}\left[P_x^{cv}(k) \pm iP_y^{cv}(k)\right]$, where + and - denote left-handed (σ_+) and right-handed (σ_-) light , and c and v denote the bottom of conduction bands and the top of valence bands, respectively. The interband transition matrix elements are the matrix elements of momentum operator between the Bloch states of conduction and valence bands $\mathbf{P}^{cv}(k) = \left\langle \Psi_{ck} \middle| \hat{\mathbf{P}} \middle| \Psi_{vk} \right\rangle$, which can be calculated by using the density functional perturbation theory as implemented in VASP. Spin-orbit coupling is not included in the calculation. Our calculations show that $P_+^{cv}(k) >> P_-^{cv}(k)$ at valley K, indicating that the K-valley only absorbs the σ_+ light. For K′ -valley, the opposite is true and it only absorbs σ_- light. We calculated the k-resolved optical circular polarization $\eta(k,\omega_{cv}) = \dfrac{\left|P_+^{cv}(k)\right|^2 - \left|P_-^{cv}(k)\right|^2}{\left|P_+^{cv}(k)\right|^2 + \left|P_-^{cv}(k)\right|^2}$, as shown in Fig. 3(c). It is found that η takes the value of +1 and -1 at K and K′ points, respectively, giving a nearly perfect valley contrasting circular dichroism. In the neighboring region of K or K′, the circular polarization η has the same sign as η(K) or η(K′), respectively, and the polarization is still rather high. Therefore, optical control of the valley freedom can be realized by using left or right handed light to excite K or K′ valley carriers, respectively. The time reversal operation transforms the K-valley and σ_+ light into the K′ -valley and σ_- light, respectively [14,42], and the valley optical selection rule is a fundamental result of the valley contrasting Berry curvatures [48].

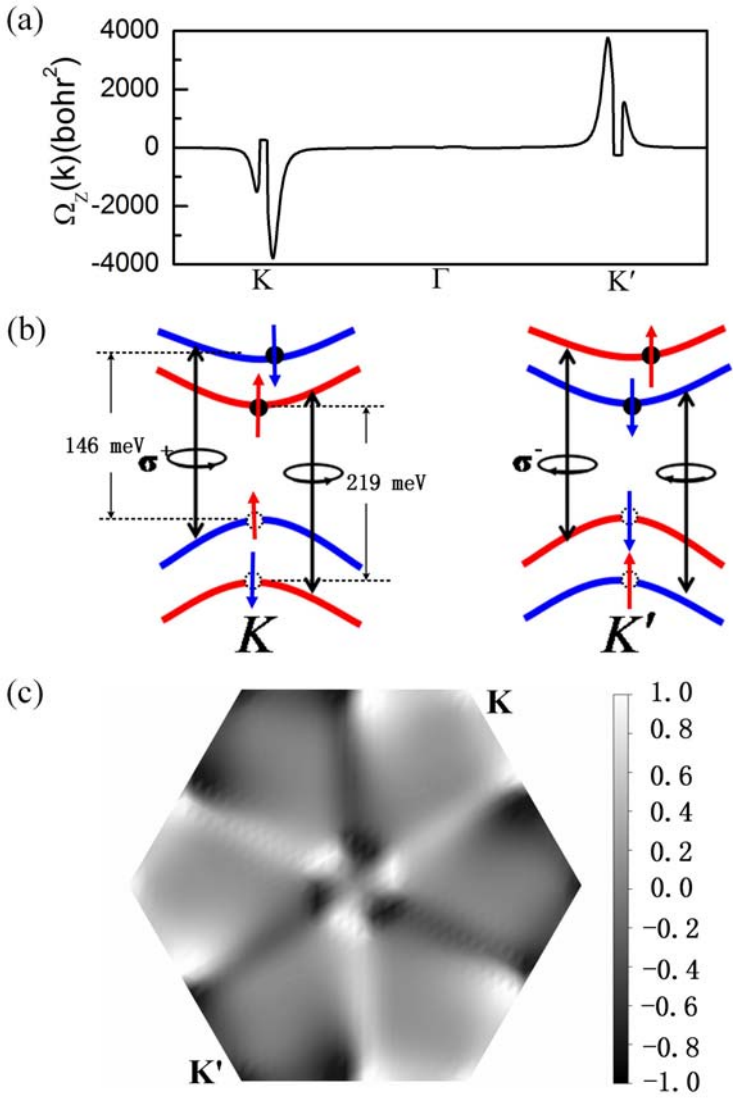

FIG. 3 (Color online). (a)The plot of the calculated z component of Berry curvature of the valence bands long the K-Γ-K′ path in the Brillouin zone. (b)The schematic plot of the band gaps between the band edges of the same spin and the valley selective optical transitions near the K and K′ Dirac valleys. The blue and red colors denote spin-down and spin-up states, respectively. The solid circles and dotted circles denote electrons and holes, respectively. The arrows through the circles denote the spin direction. (c) The plot of the k-resolved circular polarization η(k), as defined in the text.

Since, as discussed above, the proximity effect induced giant spin splittings are opposite at the inequivalent valleys, the valley and spin freedoms are locked to each other, making possible the coherent manipulation of these two freedoms. The opposite spin splittings at K and K′ valleys indicate that the valley polarization will lead to a simultaneous correlated spin polarization at the same valley, and vice versa. Such

simultaneous valley-spin polarization can be realized by optical pumping using circularly polarized photons with proper energy. As shown in Fig. 3(b), one can excite only the K-valley carriers by using σ_+ light and only the K′ -valley carriers by using σ_- light. If spin freedom is taken into account, the optical transition, which occurs only between the bands of the same spin, is not only valley dependent but also spin dependent. The spin-splittings Δ_{KV} and Δ_{KC} are different, resulting in unequal gaps between the spin-up band edges (219 meV at K point) and between the spin-down band edges (146 meV at K point), as shown in Fig. 3(b). Therefore, the 219 meV σ_+ photons, for instance, will excite only the K-valley carriers with up spin, whereas the 219 meV σ_- photons will excite only the K′ -valley carriers with down spin. By this means, the valley and spin of the excited carriers are locked with each other and the valley and spin polarization become more stable because the intervalley scattering needs to reverse the momentum and spin simultaneously. The valley circular dichroism occurs in the visible light region for TMDs while it occurs in the infrared region for Si/Bi. In the valley hall effect, the application of an in-plane electric field will lead to the separation of the K and K′ valley carriers in the transverse direction. Due to the valley-spin locking, the separation of the spin up and spin down carriers occurs simultaneously with the separation of valley carriers. The valley Hall effect and the spin Hall effect will take place concurrently.

IV. CONCLUSIONS

In conclusion, our investigations have demonstrated that by proximity effect, silicene, which has a tiny gap and zero spin splittings, can be converted into an excellent valleytronic material. The effect of Si-Bi interaction is twofold. One is to break the inversion symmetry, allowing nonzero values for Berry curvatures at the Dirac valleys. The other one is to enhance the SOC in silicene via effective hybridization with Bi states that have strong SOC, leading to giant spin splittings in the Dirac valleys. The two effects also open a sizable gap at the Dirac valleys, which is among the largest ones obtained by different means to date. Due to the presence of the time reversal symmetry in Si/Bi, it is found that the Berry curvatures at the K and K′ valleys take opposite values and accordingly the spin splittings are valley contrasting, enabling the simultaneous polarization and locking of valley and spin quantum freedoms. We have calculated the transition matrix of circular polarization and observed the perfect valley-selective circular dichroism. Therefore, with a considerable valley gap, valley contrasting Berry curvatures and giant spin splittings, Si/Bi is commensurate with the TMDs in valleytronics, to evidently exhibit Berry phase related physics and the interplay of spin and valley freedoms.

ACKNOWLEDGMENTS

The authors acknowledge the support of the National Natural Science Foundation of China (Grant No. 11274265 and No. 11474244), National Basic Research Program of China (Grant No. 2012CB921303), Furong Scholar Program of Hunan Provincial Government, and the Oak Ridge Institute for Science and Education (ORISE) HERE Program (J Z).

*xiangyang_peng@xtu.edu.cn

†jxzhong@xtu.edu.cn

[1] S. Wolf, D. Awschalom, R. Buhrman, J. Daughton, S. Von Molnar, M. Roukes, A. Y. Chtchelkanova, and D. Treger, Science **294**, 1488 (2001).

[2] A. Rycerz, J. Tworzydło, and C. W. J. Beenakker, Nat. Phys. **3**, 172 (2007).

[3] M. Ezawa, Phys. Rev. B **87**, 155415 (2013).

[4] J. Isberg, M. Gabrysch, J. Hammersberg, S. Majdi, K. K. Kovi, and D. J. Twitchen, Nat. Mater. **12**, 760 (2013).

[5] A. Popescu and L. M. Woods, Adv. Funct. Mater. **22**, 3945 (2012).

[6] Z. Zhu, A. Collaudin, B. Fauqué, W. Kang, and K. Behnia, Nat. Phys. **8**, 89 (2012).

[7] K. Eng, R. N. McFarland, and B. E. Kane, Phys. Rev. Lett. **99**, 016801 (2007).

[8] D. Xiao, W. Yao, and Q. Niu, Phys. Rev. Lett. **99**, 236809 (2007).

[9] O. Gunawan, B. Habib, E. P. De Poortere, and M. Shayegan, Phys. Rev. B **74**, 155436 (2006).

[10] C. Mai, A. Barrette, Y. Yu, Y. G. Semenov, K. W. Kim, L. Cao, and K. Gundogdu, Nano Lett. **14**, 202 (2014).

[11] D. Gunlycke, S. Vasudevan, and C. T. White, Nano Lett. **13**, 259 (2013).

[12] K. F. Mak, K. He, J. Shan, and T. F. Heinz, Nat. Nanotechnol. **7**, 494 (2012).

[13] H. Zeng, J. Dai, W. Yao, D. Xiao, and X. Cui, Nat. Nanotechnol. **7**, 490 (2012).

[14] T. Cao, G. Wang, W. Han, H. Ye, C. Zhu, J. Shi, Q. Niu, P. Tan, E. Wang, B. Liu, and J. Feng, Nat. Commun. **3**, 887 (2012).

[15] Q. H. Wang, K. Kalantar-Zadeh, A. Kis, J. N. Coleman, and M. S. Strano, Nat. Nanotechnol. **7**,

699 (2012).

[16] W.-Y. Shan, H.-Z. Lu, and D. Xiao, Phys. Rev. B **88**, 125301 (2013).

[17] D. Xiao, G. B. Liu, W. Feng, X. Xu, and W. Yao, Phys. Rev. Lett. **108**, 196802 (2012).

[18] G. Wang, Europhys. Lett. **101**, 27005 (2013).

[19] K. S. Novoselov, A. K. Geim, S. V. Morozov, D. Jiang, M. I. Katsnelson, I. V. Grigorieva, S. V. Dubonos, and A. A. Firsov, Nature **438**, 197 (2005).

[20] A. A. Balandin, Nat. Mater. **10**, 569 (2011).

[21] Z. Liu, C.-X. Liu, Y.-S. Wu, W.-H. Duan, F. Liu, and J. Wu, Phys. Rev. Lett. **107**, 136805 (2011).

[22] S. Xiao, D. Wei, and X. Jin, Phys. Rev. Lett. **109**, 166805 (2012).

[23] M. Chen, J.-P. Peng, H.-M. Zhang, L.-L. Wang, K. He, X.-C. Ma, and Q.-K. Xue, Appl. Phys. Lett. **101**, 081603 (2012).

[24] L. Chen, C. C. Liu, B. Feng, X. He, P. Cheng, Z. Ding, S. Meng, Y. Yao, and K. Wu, Phys. Rev. Lett. **109**, 056804 (2012).

[25] B. Feng, Z. Ding, S. Meng, Y. Yao, X. He, P. Cheng, L. Chen, and K. Wu, Nano Lett. **12**, 3507 (2012).

[26] L. Chen, H. Li, B. Feng, Z. Ding, J. Qiu, P. Cheng, K. Wu, and S. Meng, Phys. Rev. Lett. **110**, 085504 (2013).

[27] L. Meng, Y. Wang, L. Zhang, S. Du, R. Wu, L. Li, Y. Zhang, G. Li, H. Zhou, W. A. Hofer, and H. J. Gao, Nano Lett. **13**, 685 (2013).

[28] A. Fleurence, R. Friedlein, T. Ozaki, H. Kawai, Y. Wang, and Y. Yamada-Takamura, Phys. Rev. Lett. **108**, 245501 (2012).

[29] T. Aizawa, S. Suehara, and S. Otani, J. Phys. Chem. C. C **118**, 23049 (2014).

[30] L. Tao, E. Cinquanta, D. Chiappe, C. Grazianetti, M. Fanciulli, M. Dubey, A. Molle, and D. Akinwande, Nat. Nanotechnol. **10**, 227 (2015).

[31] J. P. Perdew, K. Burke, and M. Ernzerhof, Phys. Rev. Lett. **77**, 3865 (1996).

[32] G. Kresse and J. Furthmüller, Comp. Mater. Sci. **6**, 15 (1996).

[33] G. Kresse and J. Furthmüller, Phys. Rev. B **54**, 11169 (1996).

[34] P. E. Blöchl, Phys. Rev. B **50**, 17953 (1994).

[35] A. A. Mostofi, J. R. Yates, Y.-S. Lee, I. Souza, D. Vanderbilt, and N. Marzari, Comput. Phys.

Commun. **178**, 685 (2008).

[36] A. A. Soluyanov and D. Vanderbilt, Phys. Rev. B **83** (2011).

[37] Y. M. Koroteev, G. Bihlmayer, E. V. Chulkov, and S. Blügel, Phys. Rev. B **77**, 045428 (2008).

[38] C. C. Liu, W. Feng, and Y. Yao, Phys. Rev. Lett. **107**, 076802 (2011).

[39] L. Chen, Z. F. Wang, and F. Liu, Phys. Rev. B **87**, 235420 (2013).

[40] R. Quhe, Y. Yuan, J. Zheng, Y. Wang, Z. Ni, J. Shi, D. Yu, J. Yang, and J. Lu, Sci Rep **4**, 5476 (2014).

[41] Z.-X. Guo, S. Furuya, J.-i. Iwata, and A. Oshiyama, Phys. Rev. B **87** (2013).

[42] G.-B. Liu, D. Xiao, Y. Yao, X. Xu, and W. Yao, Chem. Soc. Rev. **44**, 2643 (2015).

[43] G.-B. Liu, W.-Y. Shan, Y. Yao, W. Yao, and D. Xiao, Phys. Rev. B **88**, 085433 (2013).

[44] H. Yuan, M. S. Bahramy, K. Morimoto, S. Wu, K. Nomura, B.-J. Yang, H. Shimotani, R. Suzuki, M. Toh, and C. Kloc, Nat. Phys. **9**, 563 (2013).

[45] W. F. Tsai, C. Y. Huang, T. R. Chang, H. Lin, H. T. Jeng, and A. Bansil, Nat. Commun. **4**, 1500 (2013).

[46] X.-L. Zhang, L.-F. Liu, and W.-M. Liu, Sci. Rep. **3**, 02908 (2013).

[47] K. Lee, W. S. Yun, and J. D. Lee, Phys. Rev. B **91**, 125420 (2015).

[48] X. Xu, W. Yao, D. Xiao, and T. F. Heinz, Nat. Phys. **10**, 343 (2014).